

Statistical Downscaling of Surface Air Temperature Projection over the Egyptian Red Sea Coast

Ahmed Abdelhamid^{1,*}, Ahmed Adel¹, Mohamed Elbessa^{1,2}, Mohamed Shaltout¹

¹Oceanography Department, Faculty of Science, Alexandria University, Alexandria, Egypt

²College of Maritime Transport and Technology (CMTT), Arab Academy for Science, Technology and Maritime Transport (AASTMT), Abu-Qir, Alexandria, Egypt

*Corresponding Author: Ahmed.Abelhamid_pg@alexu.edu.eg

ARTICLE INFO

Article History:

Received: Jan. 26, 2024

Accepted: Feb. 25, 2024

Online: Feb. 29, 2024

Keywords:

Red Sea,
Statistical downscaling,
ERA5,
GFDL,
Surface air temperature

ABSTRACT

The long-term changes in temperature and weather patterns are referred to as climate change. In particular, Egypt is susceptible to the potential consequences of climate change. Numerous ecosystems, mining resources, and touristic activities characterize the region of the Egyptian Red Sea coast (ERSC). Unfortunately, limited scientific studies have been performed on the ERSC, hence there is a large gap in knowledge that exists compared to similar ecosystems. Thus, The ERSC is an important area in which a further study of the climate projection would be highly beneficial. The recent study was implemented over five meteorological stations along ERSC (Suez, Sharm Elsheikh, Hurgada, Safaga, and Marsa Alam) with statistical analysis to describe the observed data (2011- 2021), and ERA5 reanalysis data (1979- 2021) were used together with GFDL mini-ensemble means (2011- 2100) to describe the characteristics of ERSC's future climate projection. We found that the study area will experience significant warming and increases in risks regarding heat stress. Data analysis revealed that the maximum air temperature occurred during August, while analysis of C_ERA5 (1979- 2021) showed that the annual average surface air temperature ranged from 23.3°C over Suez to 26.2°C over Sharm Elsheikh. According to C_ERA5 (1979- 2021), the historical maximum record of surface air temperature was 46.8°C, while the historical minimum record was 3.2°C. Otherwise, the SSPs' future scenarios showed a maximum increasing value of Tas as in SSP 119 (0.13°C), SSP 126 (0.36°C), SSP 434 (0.72°C), SSP 245 (1.17°C), SSP 460 (1.52°C), SSP 370 (1.85°C), and SSP 585 (2.67°C). The Suez station showed a distinct tendency from the other ERSC stations under study, which is related to the Mediterranean Sea depression (also known as the Cyprus depression) and the attraction of subtropical streams, whereas the other ERSC stations were impacted by tropical streams.

INTRODUCTION

Egypt is widely recognized as being among the nation's most susceptible to the potential consequences arising from climate change. The country's land and water resources face significant pressures due to factors, such as high population density, rapid population growth, and the widespread occurrence of unplanned urbanization. Egypt is currently facing challenges in terms of its technical capacity and community resilience in dealing with extreme weather events. It is anticipated that global warming will intensify the existing water scarcity in Egypt's arid to semi-arid climate, while also contributing to

an increase in heat waves, as well as the severity and frequency of sand and dust storms. Climate change is expected to have a significant impact on various sectors of development in Egypt, with particular emphasis on water supplies, coastal and agricultural resources, tourism, and public health. Additionally, the absence of sufficient institutional capacities in Egypt to effectively monitor and regulate these pressures will contribute to the exacerbation of their impacts (**Michel *et al.*, 2010**).

The Red Sea exhibits a maximum width of 355km in its southern half, while its minimum width is observed to be approximately 30- 40km at the Strait of Bab El-Mandab in the southern region. The Red Sea in Egypt reaches approximately 1200 kilometers, starting from the city of Suez in the northern region (latitude 30°N) and reaching the Egypt/ Sudan border in the southern region (latitude 22°N). The mean width of the Red Sea in Egypt is approximately 200 kilometers. At a latitude of 27°45'N, the Red Sea endures a division into two distinct bodies of water, forming a V-shape. To the west, it is referred to as the Gulf of Suez, while to the east, it is known as the Gulf of Aqaba (**Hereher, 2015**).

The coastline of the Red Sea on the Egyptian side exhibits a relatively narrow configuration due to the presence of a nearby mountain chain running parallel to the shoreline. The coastline is characterized by a significant presence of minor gulfs, and small beaches. The coastlines are characterized by expansive coral reef communities that exhibit both fragmentation and extension, showcasing a diverse array of marine organisms. The distribution of the population is primarily concentrated within several urban centers situated along the coastal regions, with a limited number of dispersed settlements interspersed between these cities. The Suez Canal, situated in the northern region, serves as a crucial link between the Red Sea and the Mediterranean, facilitating international maritime transportation and serving as a significant economic asset for Egypt. In the southern region, there exists a significant concentration of renowned diving locations owing to the presence of abundant and extensively varied coral and mangrove ecosystems. A substantial proportion of the local population is employed in major resort cities situated along the Red Sea. Undoubtedly, the tourism industry in the coastal area of Sinai and eastern Egypt, specifically along the Red Sea, constitutes a significant portion of Egypt's economic activities (**UNDP, 2005**).

The Red Sea is characterized by its rich and diverse ecosystem, making it a distinctive and exceptional environment (**Eladawy *et al.*, 2017**). However, the region is also confronted with the challenge of escalating habitat loss caused by the rapid expansion of unplanned urbanization, pollution, coastal landfilling, frequent occurrences of flash flooding, and the adverse impacts of tourism. The Red Sea's renowned coral communities are subject to various consequences resulting from climate change, encompassing coral bleaching due to elevated seawater temperatures, habitat degradation, and a decline in biodiversity (**Moustafa *et al.*, 1994**).

Numerous studies have determined air temperature as the key climate change measurement due to its significant impact on all sectors of life. The air temperature is a crucial climate factor that significantly impacts people's daily activities. Even a slight change in air temperature can have a noticeable effect. This increase in surface air

temperature is associated with a decrease in relative humidity. The interaction between these factors can have catastrophic consequences, particularly in the context of heat wave occurrences. This could potentially lead to higher rates of death or illness. Nevertheless, the presence of wind fields and advancements in wind technology has the potential to diminish CO₂ emissions. Changes in mean sea level pressure (SLP) can have a significant impact on climate due to its control over atmospheric circulation. Hence, this factor impacts the fluctuations in wind patterns, moisture transport, rainfall, and temperature (**Bawadekji et al., 2022**).

Most of the region is situated within the sub-tropical high-pressure belt, characterized by significant subsidence of the Hadley cell. The average daily maximum temperature in January exhibits a variation, ranging from approximately 20°C in the northernmost regions to around 29°C in the southernmost regions. In contrast, during July, these values increase to approximately 35°C in the north and 40°C in the south (**Moustafa et al., 1994**).

The Red Sea experiences a latitudinal gradient of increasing daily maximum temperature (T_{max}) from north to south due to fluctuations in solar energy. The thermal regimes of the Gulf of Suez and the Gulf of Aqaba are comparatively cooler in comparison to the southern region, which exhibits the highest thermal regime. The timing of T_{max} exhibits a discontinuous pattern within the Red Sea basin, characterized by a distinct transition occurring between the latitudes of 20 and 22°N. The rate of warming in the Red Sea is higher compared to the global ocean, with the northern region of the Red Sea experiencing a more noticeable warming trend in comparison to the southern region (**Chaidez et al., 2017**). The air temperature in the northern Red Sea exhibits its lowest values throughout the year, with recorded temperatures ranging from 6 to 39°C at the Suez Canal and from 13.5 to 42°C at Jeddah. There is a noticeable and rapid rise in temperature as one moves towards the southern latitudes below 26°N. The region with the highest temperatures in the Red Sea is located between the latitudes of 20 and 16°N (**Moustafa et al., 1994**).

According to **Tonbol et al. (2019)** the monthly mean air temperature at Safaga Harbour during the period 2007- 2017 ranged between 16.77 and 33.57°C, with an overall average of 26°C, while the mean monthly air temperature anomaly ranged between -2.89 and +2°C with a very slight trends of increase of +0.00004°C/ month and +0.01°C/ year.

Despite the existence of numerous prior investigations aimed at examining the present state of air temperature along the ERSC, a recurring issue in previous analyses of the recent air temperature appears to be the limited duration of these studies. Therefore, it was imperative to conduct more extensive and enduring investigations to acquire a more profound comprehension of the recent alterations in air temperature. However, it was worth noting that there was a scarcity of climatic modeling studies conducted in the ERSC region. Most of these studies relied on the analysis of regional climatic models. The utilization of statistical downscaling in the analysis will reinforce the findings of the previous modeling efforts and facilitate a discourse on enhancing future studies by

addressing uncertainties. One potential method for addressing this issue entailed employing a recently developed technique that has arisen from the examination of 43 years' worth of contemporary air temperature, coupled with the statistical extrapolation to the year 2100. Our initial objective was to address the issues. Upon resolving these problems, we can figure out whether the ERSC region experiences a higher or lower degree of warming in comparison to its neighboring regions. Therefore, the present research findings were anticipated to generate significant interest and provide valuable insights for policymakers and decision-makers in formulating efficacious strategies and policies to address the challenges posed by shifting climatic conditions.

MATERIALS AND METHODS

1. Data and methods of analysis

The present study implemented statistical downscaling approaches to anticipate the future air temperature over the northern region of the Egyptian Red Sea Coast (ERSC). Five locations within the study area, including Suez, Sharm Elshikh, Hurgada, Safaga, and Marsa Alam, were assigned to represent numerous climate conditions and a range of human activities. These locations were arranged from north to south, as shown in Fig. (1).

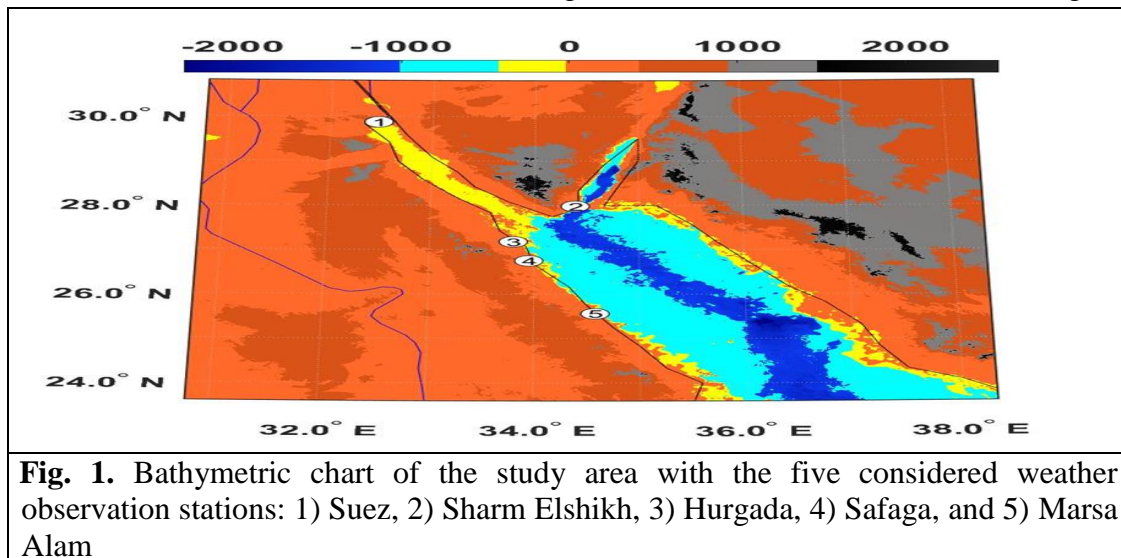
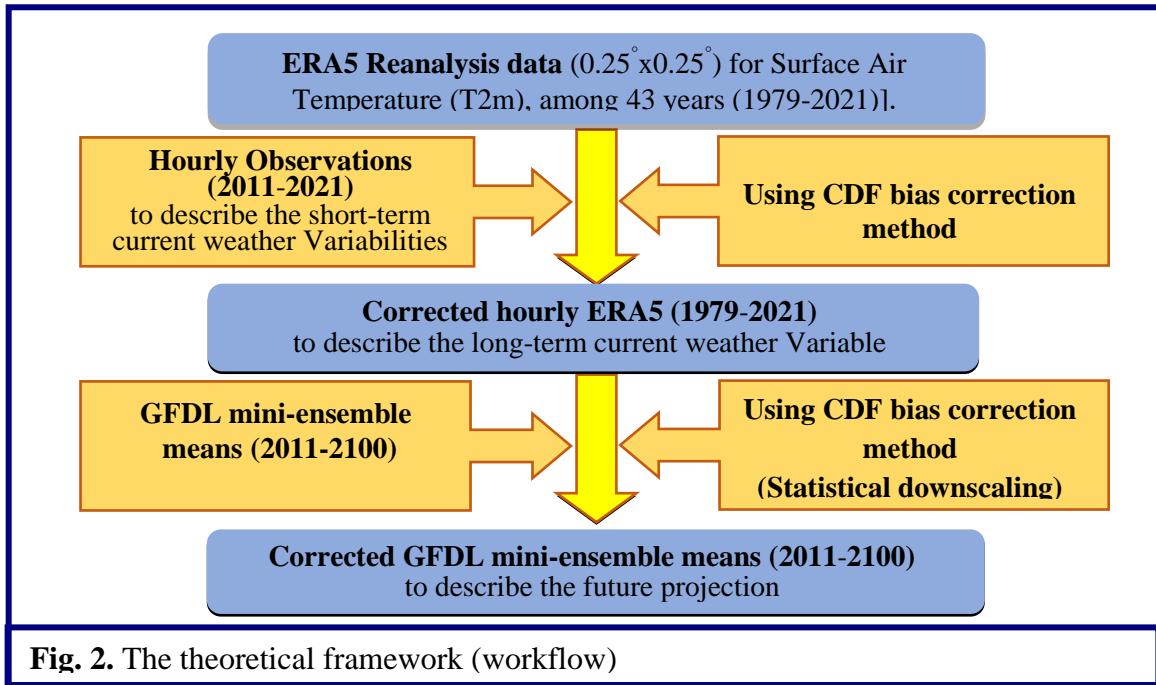


Fig. 1. Bathymetric chart of the study area with the five considered weather observation stations: 1) Suez, 2) Sharm Elshikh, 3) Hurgada, 4) Safaga, and 5) Marsa Alam

Fig. (2) illustrates the theoretical framework of the study, where the first step involves utilizing the observed data to depict the existing short-term fluctuations in air surface temperature (T2m) from 2011 to 2021. Secondly, the current research validates the use of ERA5 in accurately capturing the mentioned atmospheric studied parameter. Thirdly, applying bias correction involves aligning the cumulative distribution function (CDF) of the observed data with the CDF of the ERA5 database at the specific station level, where the current long-term surface air temperature was described using 43 years (1979- 2021) of ERA5 data, which was experiencing bias removal. Finally, the future scenarios of the ERSC were projected using statistical downscaling for the Geophysical Fluid Dynamics Laboratory (GFDL) mini-ensemble means. This method was employed to analyze the future projection over the study area. This approach used Coupled Model

Inter-comparison Project phase six (CMIP6) to project temperature extremes globally and regionally the latest version of CMIPs, known as CMIP6, has undergone significant advancements in parameterization, physics, numerical methods, and configurations. It includes socioeconomic scenarios known as shared socioeconomic pathways (SSPs), making it more reliable in terms of climate projection. The improvements in CMIP6 include additional models and experiments, higher horizontal resolution, and lower biases compared to the elder versions (Hamed *et al.*, 2023).



2. Data used

2.1. Observed data

Five Automated Weather Observing Systems (AWOS) along the ERSC were used to collect T2m at Suez, Sharm Elsheikh, Hurgada, Safaga, and Marsa Alam, as shown in Table (1). AWOS was installed and maintained according to World Meteorological Organization (WMO) regulations. Where T2m is calibrated to WMO standard height 2m, these five stations are well spatially distributed along the ERSC and extended from 2011 to 2021 on an hourly basis, with an average missed data along the study area ranging from 5.5 to 7%, which considered an acceptable percentage.

Table 1. Elevations and positions of meteorological working stations. The identification numbers (IN) 1 to 5 are also included in association with Fig. (1)

Station name	IN	Height above sea level (m)	Geographic position		International station number
			Latitude (N)	Longitude (E)	
Suez	1	13.48	29° 52' 14"	32° 28' 30"	62450
Sharm ElSheikh	2	50	27° 58' 38.24"	34° 23' 41.82"	62460
Hurgada	3	14	27° 10' 43"	33° 48' 2.99"	62463
Safaga	4	18	26° 45' 2"	33° 57' 10"	62466
Marsa Alam	5	77	25° 33' 25.56"	34° 35' 1.32"	62470

2.1.2 ERA5 database

Hourly data from 1979 to 2021 were obtained freely from the European Eyes on Earth (Copernicus) website:

(<https://cds.climate.copernicus.eu/cdsapp#!/dataset/reanalysis-era5-single-levels?tab=form>).

ERA5 data, which is distributed by the Copernicus Climate Change Service (C3S) and produced by the European Center for Medium-Range Weather Forecast (ECMWF), were intended to improve on the success of the earlier issues (e.g., ERA-Interim and ERA40) and improve atmospheric parameters (**Hersbach *et al.*, 2020**), with a finer spatial grid of $0.25^{\circ} \times 0.25^{\circ}$ and temporal hourly resolution. This data, after validation with observations, is used to analyze long-term trends of the studied atmospheric variable. Moreover, this data is used to statistically downscale global climate simulations over the five studied stations.

2.1.2 Modeled data (2010- 2100)

The GFDL climate model simulation of surface air temperature T_{as} , for the period 2010- 2100 was extracted from three model realizations: GFDL-CM3 (**Griffies *et al.*, 2011**), GFDL-ESM2M (**Dunne *et al.*, 2012**), and GFDL-ESM2G (**Dunne *et al.*, 2013**). These simulations are available on the GFDL website (<https://aims2.llnl.gov/search/?project=CMIP6>) through CMIP6 emission scenarios with a coarse grid resolution of $2^{\circ} \times 2^{\circ}$.

2.1 Methods of analysis

2.1.1 Observed data statistical analysis

The observed data for T_{2m} during the period 2011- 2021 were subjected to statistical analysis (mean, standard deviation, minimum, and maximum) to investigate its temporal variation on an hourly, daily, monthly, and annual basis.

2.1.2 ERA5 efficiency test, bias removal, and trend analysis

Direct comparisons of the hourly-observed data and ERA5 are used to test the efficiency of ERA5 over the studied five stations. Moreover, the f- and t-tests are used to examine whether ERA5 and the observations display equal means and variances (come from the same population) or not at a 95% significance level. In addition to that, ERA5 databases are subjected to CDF bias correction between ERA5 and observation over 2011- 2018 (calibration period), whilst the years from 2019 to 2021 are used for the validation processes between ERA5 and observation.

The present strategy for bias correction is to match the CDF of the observations to the CDF of the ERA5 database at the station level. The spatial mismatch between the point observation and the ERA5 grid cell is a challenge in this bias correction. Only stationary points are analyzed in the current study. Therefore, our strategy may make use of this bias correction. Moreover, the technique of calibration and validation is used to test the efficiency of ERA5 to describe the air temperature over the studied five stations. This strategy was used by many researchers. **Anagnostou *et al.* (1999)** used the CDF strategy to statistically adjust the satellite microwave for monthly rainfall estimates. Furthermore, **Wood *et al.* (2002)** used the CDF technique for long-range hydrologic forecasting. **Reichle and Koster (2004)** used this strategy to match the CDF between satellite retrievals and model soil moisture. Finally, **Bawadekji *et al.* (2022)** used this

strategy to match the CDF between observed and ERA5 atmospheric parameters along the Red Sea Saudi Arabia coast.

A boxplot analysis was used to visually show the distribution of C_ERA5 (ERA5 after bias removal) by presenting the data quartiles and averages on a monthly basis. Box plots display: 1) the minimum value, 2) the lower quartile, 3) the median, 4) the upper quartile, and 5) the maximum value, as stated by **Williamson *et al.* (1989)**.

A linear trend analysis, based on the ERA5 after correction (hereafter, C_ERA5) from 1979 to 2021, was used to characterize the current long-term surface air temperature along ERSC over the studied five stations. Moreover, the non-parametric Mann-Kendall test (**Mann, 1945; Kendall, 1975**) was used to detect monotonic trends in C_ERA5 to examine whether C_ERA5 followed a significant (monotonic) trend or not. The limitations of the Mann-Kendall test are frequently associated with data that has serial correlation. The term "serial correlation" refers to the relationship between two variables with various lag periods. Each observation is independent of the other if the serial correlation of a variable is 0. If the serial correlations tend to be one, the observations are serially correlated, and the Mann-Kendall test will not identify monotonic trends, to avoid this limitation in the studied atmospheric parameters, the trend-free pre-whitening technique was used (**Wang *et al.*, 2020**).

In addition, the studied atmospheric parameter was analyzed to establish the dates of the historically most extreme events (date of the maximum/minimum values) based on the C_ERA5 hourly data.

Furthermore, by splitting the complete range of the hourly data into a limited number of intervals (bins equal to 1 °C for T2m), the histogram was utilized to depict the probability density of hourly data values. The horizontal axis indicated the probable range of daily data values in the current study, while the vertical axis reflected the frequency of occurrence [%]. The percentage of occurrences during the extreme events (highest and lowest) was calculated according to **Elbessa *et al.* (2021)**, as mentioned in Equation 1.

$$\text{The percentage of occurrences} = \text{Mean} \pm 2 \times \text{Standard Deviation} \quad (1)$$

2.1.3 Statistical downscaling for future projection

The results of the three GFDL realizations are averaged to calculate the GFDL mini-ensemble mean from 2010 to 2100. Then, the CDF of observation is matched with the CDF of the GFDL mini-ensemble mean under a control period (2010- 2021) to describe a simple statistical model for bias removal from GFDL mini-ensemble mean simulation. This statistical model is used to statistically downscale the studied atmospheric parameters up to 2100 under different future SSPs scenarios. The future projections under various SSPs scenarios were calculated using the 30-year running average. The statistically downscaled GFDL mini-ensemble mean simulations (S_D_GFDL mini-ensemble mean) were used to calculate atmospheric future projection with better accuracy and validity along ERSC. In which statistical downscaling is a technique used to bridge the gap between global climate models and local weather conditions, increase spatial resolution, enhance local climate information, improve projection of extreme events, integrate

observations and model outputs, in addition to the flexibility and accessibility of it which is crucial for decision support and planning.

RESULTS AND DISCUSSION

1. Observed data

Table (2) shows annual, monthly, and hourly characteristics for T2m based on hourly observed data during the period 2011- 2021 over Suez, Sharm Elsheikh, Hurgada, Safaga, and Marsa Alam.

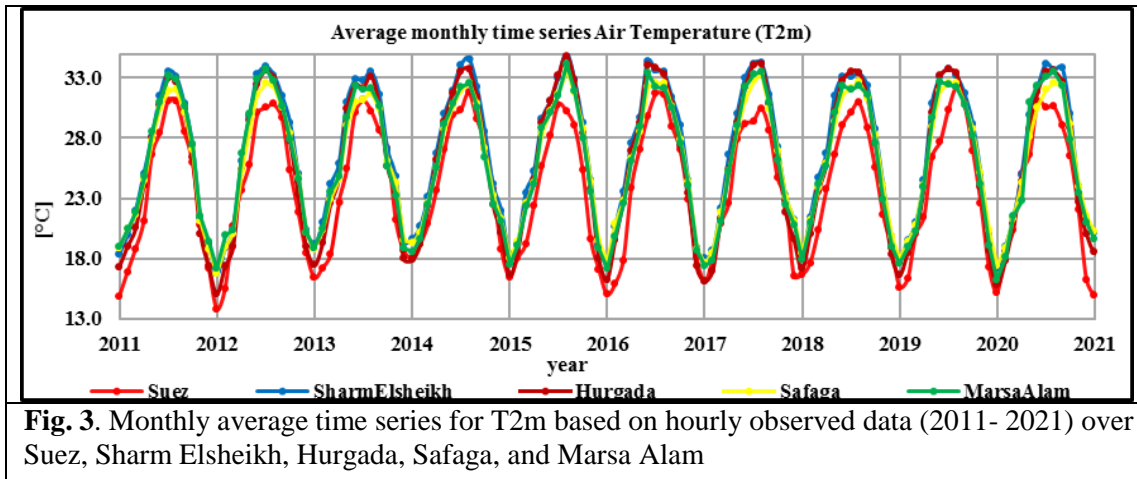
Table 2. Annual, monthly, and hourly characteristics for T2m based on hourly observed data during the period 2011 to 2021 over Suez, Sharm Elsheikh, Hurgada, Safaga, and Marsa Alam.

Station		Max	Min
Suez	Annual	2011 25.05	2018 23.48
	Monthly	Aug. 31.00	Jan. 15.72
	Hourly	at 1500 28.31	at 0500 20.34
Sharm Elsheikh	Annual	2021 27.38	2011 25.76
	Monthly	Aug. 33.77	Jan. 18.33
	Hourly	at 1300 30.86	at 0300 23.11
Hurgada	Annual	2018 26.39	2011 24.95
	Monthly	Aug. 33.49	Jan. 16.81
	Hourly	at 1200 30.82	at 0400 21.28
Safaga	Annual	2018 26.57	2011 25.41
	Monthly	Aug. 32.60	Jan. 18.27
	Hourly	at 1300 28.28	at 0500 23.57
Marsa Alam	Annual	2012 26.38	2020 21.51
	Monthly	Aug. 32.86	Jan. 17.79
	Hourly	at 1100 28.80	at 0300 22.54

1.1 Monthly time series

The monthly average time series for T2m based on hourly observed data from 2011 to 2021 over Suez, Sharm Elsheikh, Hurgada, Safaga, and Marsa Alam are shown in Fig. (3). Where T2m data analysis illustrated that January 2012 was the coldest month

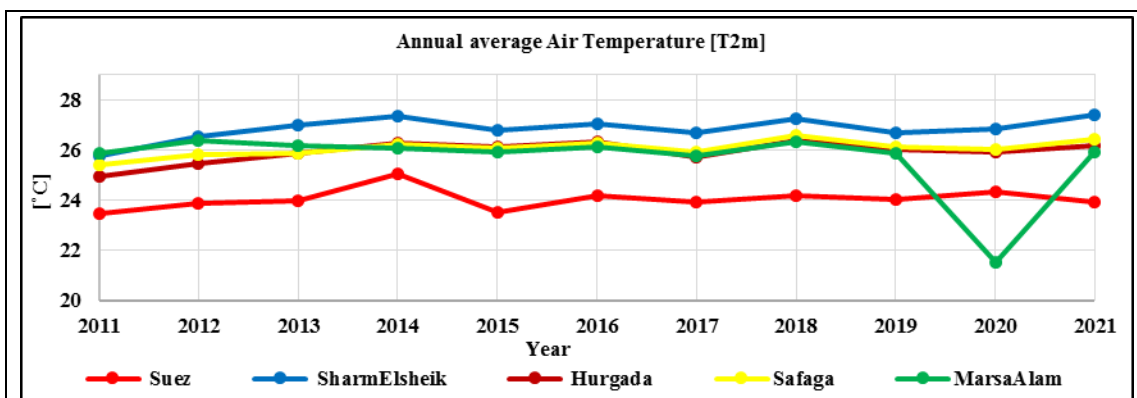
during the study period at Suez, Sharm Elsheikh, Hurgada, and Safaga, with a value of 13.7, 16.7, 15.1, and 16.8°C, respectively. While at Marsa Alam it was in January 2020 with a value of 16.2°C. On the other hand, August 2015 was the warmest month during the study period at Sharm Elsheikh, Hurgada, Safaga, and Marsa Alam with a value of 35.1, 34.8, 33.6, and 34.2°C, respectively. While at Suez it was in August 2019 with a value of 32.2°C.



1.2 Annual time series

Annual average time series for T2m based on hourly observed data from 2011 to 2021 over Suez, Sharm Elsheikh, Hurgada, Safaga, and Marsa Alam are shown in Fig. (4). Where T2m data analysis revealed that 2018 was the hottest year during the study period at Hurgada and Safaga, while at Suez, Sharm Elsheikh, and Marsa Alam, it was in 2011, 2021, and 2012, respectively. Likewise, 2011 was the coldest year at Sharm Elshikh, Hurgada, and Safaga, while at Suez and Marsa Alam it was in 2018 and 2020, respectively.

In general, the annual average T2m along the ERSC reached its maximum at Sharm Elsheikh, Safaga, Hurgada, Marsa Alam, and Suez with a value of 27.39, 26.57, 26.39, 26.38, and 25.06°C, respectively. Otherwise, T2m annual average reached its minimum at Marsa Alam, Suez, Hurgada, Safaga, and Sharm Elsheikh with a value of 21.51C, 23.48, 24.95, 25.41, and 25.76°C, respectively.



1.3. Annual (surface air temperature monthly average) and hourly cycle

The annual cycle (surface air temperature monthly average) is described in Table (2) and Fig. (5). The annual T2m cycle has a maximum value in August and a minimum value in January along the studied five stations. The amplitude of the T2m annual cycle exhibited a variation (MAX T2m - MIN T2m) from 14.33 at Safaga to 16.69°C at Hurgada.

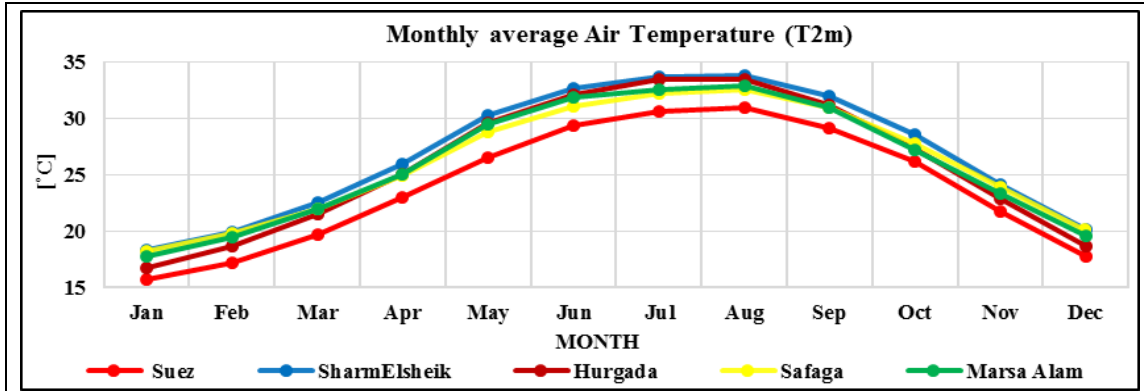


Fig. 5. Observed short-term monthly means (Annual cycle) for T2m based on hourly observed data (2011- 2021)

For the hourly cycle, as described in Table (2) and Fig. (6), the amplitude of the daily T2m cycle over Hurgada (9.54°C) was much higher than that over Suez (7.97°C), Sharm Elsheikh (7.75°C), Marsa Alam (6.26°C), and Safaga (4.71°C).

In detail, the T2m showed a diurnal cycle along ERSC, whereas the minimum value occurred between 0300- 0500 and the maximum values occurred between 1100- 1500. T2m daily range showed its maximum value over Hurgada and its minimum value over Safaga.

The most notable result of this analysis was that of the observed short-term hourly data which showed that Suez station has a different pattern than other stations due to the Mediterranean Sea depression (also known as the Cyprus depression) and the attraction of subtropical streams, whereas the other ERSC stations were impacted by tropical streams. Other notable result of this analysis was that there is non-significant trend of T2m during the study period along the ERSC.

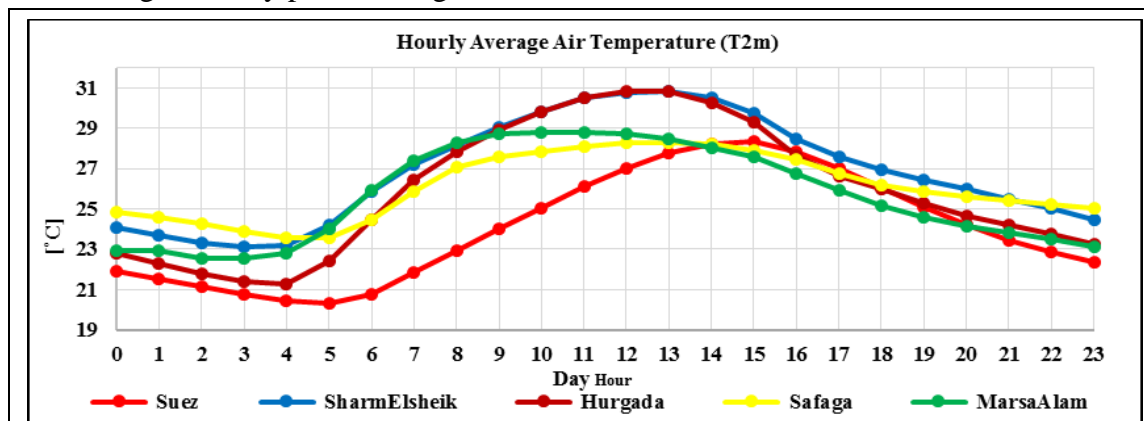


Fig. 6. Observed short-term hourly means (Daily cycle) for the parameters under study based on hourly observed data (2011- 2021)

2 ERA5 reanalysis data

2.1 ERA5 calibration

To evaluate the conveniently of using ERA5 in describing T2m over Suez, Sharm Elsheikh, Hurgada, Safaga, and Marsa Alam, we carried out a comparison between observations data and ERA5 datasets covering the observation period from 2011 to 2021, where results represented in Table (3). In general, ERA5 reanalysis data have closely matched the observations over the five studied stations. ERA5 lower estimate T2m observation at Suez, Sharm Elsheikh, Hurgada, and Safaga by 1.4, 0.3, 1.7, 0.6°C, respectively. While showing an identical average value to the observed T2m over Marsa Alam.

At a 99% significance level, statistical tests (t- and f-tests) indicated that ERA5 and observed datasets of T2m values come from two equal distributions of mean and variance.

Table 3. Comparison analysis between observed and ERA5 T2m over Suez, Sharm Elsheikh, Hurgada, Safaga, and Marsa Alam. (n = number of observations, r = correlation coefficient in percentage)

Variable		n	r [%]	Minimum	Maximum	Annual mean standard deviation	
Surface air temperature (T2M, °C)	Suez	Observed	96432	87.6	1.2	42.5	24.04±6.4
		ERA5			7.6	41	22.6±6
	Sharm Elsheikh	Observed	91645	96.7	2	46	26.85±6.5
		ERA5			8.2	42.4	26.52±6.4
	Hurgada	Observed	92766	96.5	6	46	25.9±7.1
		ERA5			8.5	37.7	24.21±5.7
	Safaga	Observed	96332	97.1	10	42.7	26.06±5.6
		ERA5			10.1	38.2	25.5±5.5
	Marsa Alam	Observed	71644	96.3	5	45	25.8±6.23
		ERA5			6.3	41.4	25.8±6.3

2.2 ERA5 bias correction

To remove ERA5 bias, CDF bias correction is applied to match the CDF of the ERA5 to the CDF of the observation from 2011 to 2021, as seen in Fig. (7). This technique preserves the nature of the data by adjusting the bias to zero and saves the correlation values as the same values. This strategy was applied for the long-term ERA5 database to calculate the corrected ERA5 reanalysis data (C_ERA5) over the five studied stations. Fig. (7) proves the current results that ERA5 reanalysis data more reasonably simulates T2m over all stations as the three curves of observations, ERA5, and C_ERA5 are so close.

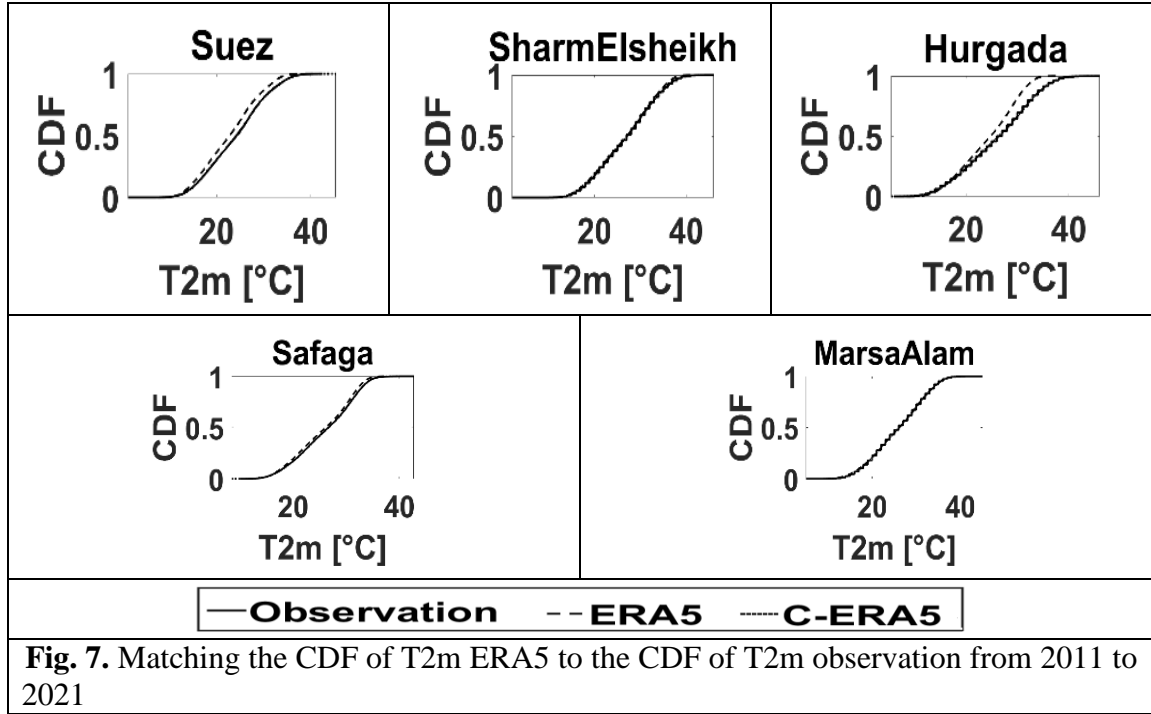


Fig. 7. Matching the CDF of T2m ERA5 to the CDF of T2m observation from 2011 to 2021

2.3 ERA5 validation

In this section, the validation was used to evaluate whether a calculated statistical model during the calibration period was appropriate or not. Table (4) shows the comparison between ERA5 and C_ERA5 in describing T2m over the studied five stations. The C_ERA5 showed a lower bias with the observation than ERA5 did. However, the correlation between the C_ERA5 and observation showed a similar value as ERA5 did. Therefore, using C_ERA5 is useful and valid to describe the long-term current weather characteristics and gives a better weather description of the studied stations.

Table 4. The comparison between ERA5 and C_ERA5 in describing the weather characteristics over the studied five stations for the validation period (2011- 2021)				
Variable	Station	Validation	r [%]	Bias
Surface air temperature (T2M, °C)	Suez	Observed, ERA5	0.878	1.35
		Observed, Corr_ERA5	0.877	0.00
	Sharm Elsheikh	Observed, ERA5	0.967	0.325
		Observed, Corr_ERA5	0.967	0.000
	Hurgada	Observed, ERA5	0.965	1.72
		Observed, Corr_ERA5	0.965	0.00
	Safaga	Observed, ERA5	0.452	0.532
		Observed, Corr_ERA5	0.448	0.000
	Marsa Alam	Observed, ERA5	0.963	0.051
		Observed, Corr_ERA5	0.963	0.000

2.4 Corrected ERA5 statistical analysis

2.4.1 Boxplot analysis

T2m exhibited a significant monthly variation, where the 75th percentile of T2m occurred in August over all the studied stations, as seen in Fig. (8) along the ERSC. Generally, the outliers' values for T2m are mostly above the upper quartile, values as illustrated in Fig. (8).

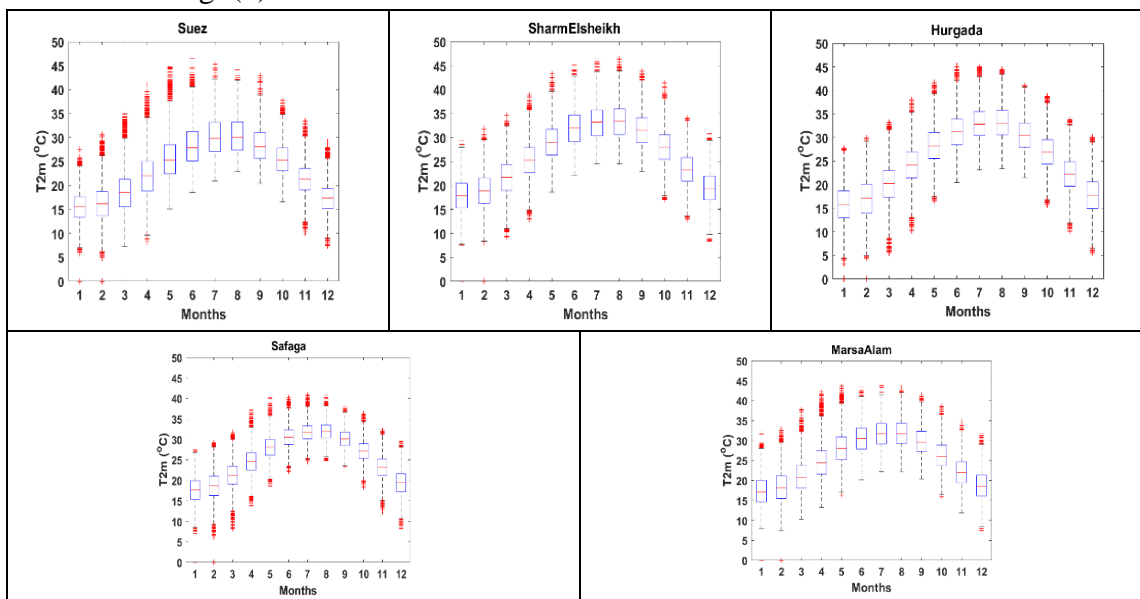


Fig. 8. Boxplot analysis for T2m on a monthly basis.

The red line in the interior of the box shows the median value. The lower and upper endpoints of the box show the 25th and 75th percentiles. The distance from the 25th to the 75th percentiles is abbreviated by IQR. An arm extending out of each side of the box shows variability outside the upper and lower quartiles as each arm extends no more than 1.5 times the IQR. + sign shows the value of the outlier

2.4.2 Annual trend analysis

C_ERA5 datasets (1979- 2021) demonstrated that the annual average of T2m over the studied stations revealed a significant spatial variation, as noticed in Table (5). In the same context, the T2m experienced a positive monotonic trend over the five studied stations. In detail for the period from 1979 to 2021, the warming trend along the study area showed a spatial variation with a positive trend over the ERSC ranging from 0.04 (Sharm Elsheikh, Safaga, and Marsa Alam) and 0.05°C (Suze and Hurgada), as seen in Table (5).

Table 5. Long- term annual mean and trend analysis for corrected ERA5 T2m over studied stations from 1979 to 2021. The non-parametric (Mann-Kendall test) is used to detect monotonic trends in corrected ERA5 to examine whether or not C_ERA5 follows a significant (monotonic) trend

Variable		Annual mean ± standard deviation	Trend (decade-1)	Significant (monotonic) trend
Surface air temperature (T2M, °C)	Suez	23.3 ± 6.4	0.05°C	Yes
	SharmElsheikh	26.2 ± 6.6	0.04°C	Yes
	Hurgada	25.1 ± 7.2	0.05°C	Yes
	Safaga	25.4 ± 5.8	0.04°C	Yes
	MarsaAlam	25.1 ± 6.4	0.04°C	Yes

2.4.3 Historical days

T2m dataset during the study period revealed that the highest temperature along the study area recorded a peak on 29th July 2000 at 1200 over Sharm Elsheikh (46.8°C), on 21st June 2010 at 1600 over Suez (46.5°C), on 5th June 2016 at 1100 over Hurgada (45.4°C), on 2nd July 1995 at 1200 over Marsa Alam (43.9°C), and on 30th July 2000 at 1300 over Safaga. On the other hand, the lowest temperature along the study area was recorded on 31st January 1981 at 0400 over Hurgada (3.2°C), on 10th February 1992 at 0300 over Suez (4.8°C), on 5th February 1992 at 0400 over Safaga (6.2°C), on 28th December 1986 at 0400 over Marsa Alam (7.4°C), and on 29th January 2000 at 0400 over Sharm Elsheikh (7.5°C).

2.4.4 The probability of occurrence

The highest occurrence percentage of hourly T2m is 5.9 (26- 27°C), 5.5 (29- 30°C), 5.2 (27- 28°C), 6.8 (29- 30°C), and 5.8% (26- 27°C) over Suez, Sharm Elsheikh, Hurgada, Safaga, and Marsa Alam, respectively. The percentage of occurrences during the hottest hours (mean+2*standard deviation) was 1.3 (>36.1°C), 0.9 (>39.4°C), 0.6 (>39.5°C), 0.2 (>37°C), and 0.8% (>37.9°C) over Suez, Sharm Elsheikh, Hurgada, Safaga, and Marsa Alam, respectively. While the percentage of occurrences during the coldest hours (mean-2*standard deviation) was 0.9 (<10.5°C), 1.1 (<13°C), 1.6 (<10.7°C), 2 (<13.8°C), and 1.1% (<12.3°C) over Suez, Sharm Elsheikh, Hurgada, Safaga, and Marsa Alam, respectively, as shown in Fig. (9).

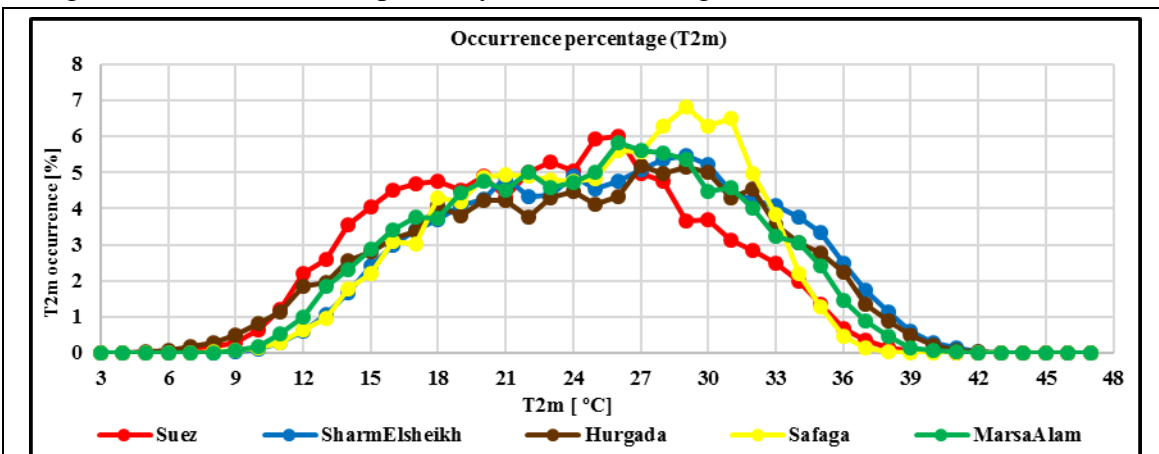


Fig. 9. The occurrence percentage of the parameters under study based on hourly corrected ERA5 data (1979- 2021) along the study area

3. Statistical downscaling for future projection

This section examined the results of GFDL mini-ensemble mean simulations using various SSPs scenarios for Tas (surface air temperature in the future scenarios).

3.1 GFDL model bias correction under the control period (2011- 2021)

As seen in Table (6), the GFDL mini-ensemble mean overestimated Tas over Suez, Sharm Elsheikh, Hurgada, Safaga, and Marsa Alam by 2.86- 17.25°C.

Table 6. Performance of GFDL mini-ensemble mean in the control period (2011- 2021) variables over Suez, Sharm Elsheikh, Hurgada, Safaga, and Marsa Alam: only the SSP 2.6 scenario is used

Station	Suez	Sharm Elsheikh	Hurgada	Safaga	Marsa Alam
Annual GFDL mini-ensemble mean - Annual Corrected ERA5 (Tas, °C)	2.86	5.07	5.98	5.86	17.25

As shown in Fig. (10), a simple statistical model was created by comparing the CDF of C_ERA5 with the GFDL mini-ensemble means under a control period (2011-2021) for the various SSPs scenarios to overcome the underestimates/ overestimates of the GFDL mini-ensemble mean that are incomparable with C_ERA5. Only SSP 126 was conducted for bias adjustment as an example. However, due to the resemblance with SSP 126 during the control period, the bias correction for SSP 119, SSP 126, SSP 434, SSP 245, SSP 460, SSP 370, and SSP 585 was not displayed.

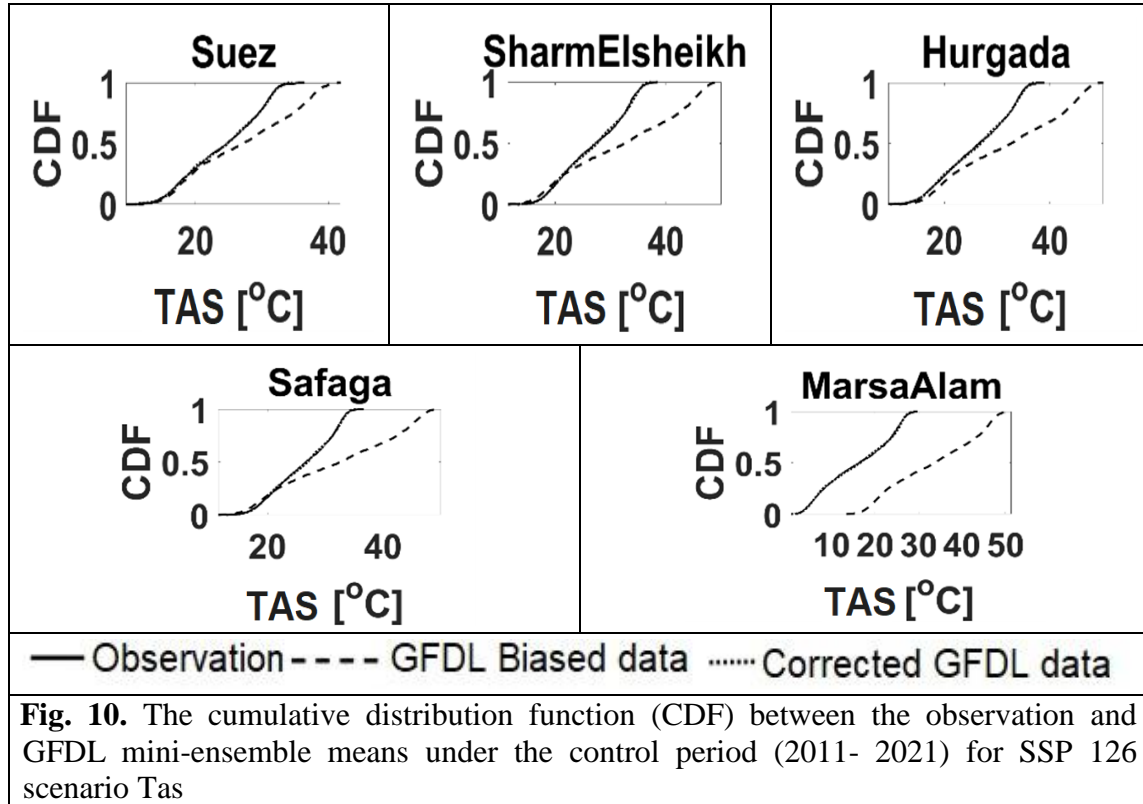


Fig. 10. The cumulative distribution function (CDF) between the observation and GFDL mini-ensemble means under the control period (2011- 2021) for SSP 126 scenario Tas

3.2 Future atmospheric projection (2030- 2100)

Based on the developed statistical model, which was obtained by matching the CDF of the GFDL mini-ensemble mean with the CDF of the observation during the control period (2011- 2021) for the various SSPs scenarios, the GFDL mini-ensemble mean at each site for the period 2011- 2100 was subjected to bias removal to calculate S_D_GFDL mini-ensemble mean simulations (statistically downscaled GFDL mini-ensemble mean). For each site along the ERSC, calculated S_D_GFDL mini-ensemble means were utilized to compute the atmospheric future projections with better accuracy.

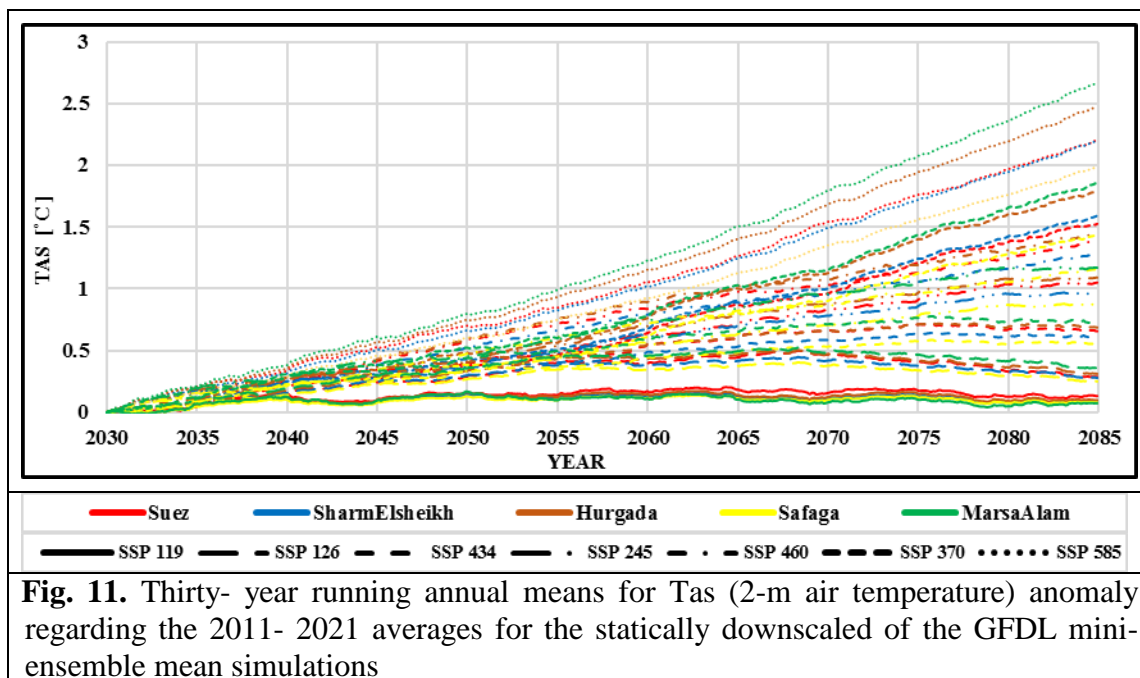
The 30-year running average was used to create future projections for the investigated parameters through the four SSP's future scenarios.

S_D_GFDL mini-ensemble means of projected Tas scenarios up to 2100 denotes significant warming along the ERSC notably for the SSP 585 scenario at Marsa Alam, as shown in Fig. (11). The projected warming at the end of the current century (with reference to the 2011- 2021 averages value) described a positive trend which ranged between 0.07°C at Marsa Alam and 0.13°C at Suez under the SSP 119 scenario, 0.25°C at Safaga and 0.36°C at Marsa Alam under the SSP 126 scenario, 0.55°C at Safaga and 0.72°C at Marsa Alam under the SSP 434 scenario, 0.88°C at Safaga and 1.17°C at Marsa Alam under the SSP 245 scenario, 1.16°C at Safaga and 1.52°C at Marsa Alam under the SSP 460 scenario, 1.44°C at Safaga and 1.85°C at Marsa Alam under the SSP 370 scenario, and 1.99°C at Safaga and 2.67°C at Marsa Alam under the SSP 585 scenario, as mentioned in Table (7).

Table 7. The projected surface air temperature (Tas) trend at the end of the current century (with reference to the 2011- 2021 averages value) over studied stations							
Station	ssp119	ssp126	ssp434	ssp245	ssp460	ssp370	ssp585
Suez	0.13	0.29	0.66	1.05	1.39	1.53	2.2
Sharm Elsheikh	0.09	0.28	0.61	0.97	1.28	1.6	2.2
Hurgada	0.1	0.31	0.69	1.09	1.44	1.8	2.48
Safaga	0.08	0.25	0.55	0.88	1.16	1.44	1.99
Marsa Alam	0.07	0.36	0.72	1.17	1.52	1.85	2.67

According to IPCC 2023 (P. 12), the best estimates for the different scenarios were 1.4 (SSP 119), 1.8 (SSP 126), 2.7 (SSP 245), 3.6 (SSP 370), and 4.4°C (SSP 585) (**Calvin *et al.*, 2023**). Comparable to IPCC 2023 estimates, the current study results showed that the warming trend through various SSPs scenarios has a significant decrease than the global average by 84, 71, 56, 48, and 39% partially for SSP 119, SSP 126, SSP 245, SSP 370, SSP 585, respectively. This decrease may be due to the lower emission over the studied area than the global, where all of Africa is responsible for about 4% of global emissions according to 2018 Global Greenhouse Gas Emissions Data issued by the United States Environmental Agency.

Generally, the future warming uncertainty is 1.05°C. 85% of this uncertainty is related to scenario design, while 15% of this uncertainty is related to regional variation. These values show that management actions should prioritize reducing emissions.



According to these findings significant warming may have many implications along the ERSC such as, sea level rise which leads to coastal erosion, change in precipitation patterns and increase evaporation rates, impact on marine ecosystem and biodiversity, risk to human health and well-being. Decision makers should implement various adaptation and mitigation strategies in the region to cope with these implications.

CONCLUSION

Unfortunately, only a limited number of scientific studies have been published regarding the climate along the ERSC. These limited studies specifically examined dynamical downscaling, emphasizing the necessity for additional endeavors, particularly in the realm of statistical downscaling, to improve our comprehension of the present and future climate. Hence, constructing a precise statistical downscaling system to replicate the climate along the ERSC would be highly advantageous in delivering more reliable information to decision-makers. The present study offered a comprehensive analysis to address the existing deficiency in climate forecasting. Furthermore, this paper provided a comprehensive and detailed analysis of the atmosphere in the study area based on recent in situ observed data.

Observation data (2011- 2021), and ERA5 reanalysis data (1979- 2021) were used together with GFDL mini-ensemble means (2011- 2100) to describe the characteristics of recent surface atmospheric fluctuation along the ERSC together with building a statistical downscaling model to project the future climatic change.

Data analysis revealed that the maximum air temperature occurred during August. While analysis of C_ERA5 (1979- 2021) showed that the annual average surface air temperature ranges from 23.3°C over Suez to 26.2°C over Sharm Elsheikh.

Depending on C_ERA5 (1979- 2021), the historical maximum record of surface air temperature was 46.8°C. In the same context, the historical minimum record of air temperature was 3.2°C.

ERA5 lower estimate in T2m along the study area by 0.8°C. Moreover, ERA5 closely describes T2m along ERSC with a significant correlation of 94.8% (n~89764). Generally, ERA5 reanalysis data simulated efficiently T2m over all stations. Moreover, the C_ERA5 dataset indicates that the study area experiences significant warming trends together with a positive monotonic increase in T2m.

In the control period (2011- 2021), the GFDL mini-ensemble means overestimates in Tas. This indicates the importance of using bias removal techniques CDF to correct the GFDL mini-ensemble mean to be valid for the studied area.

Further CDF techniques were used to statistically downscale GFDL mini-ensemble mean simulations along the ERSC. We predict that the study area will experience significant warming and increases in risks regarding heat stress up to 2100.

The SSPs' future scenarios show a maximum increasing value of Tas, such as in SSP 119 (0.13°C), SSP 126 (0.36°C), SSP 434 (0.72°C), SSP 245 (1.17°C), SSP 460 (1.52°C), SSP 370 (1.85°C) and SSP 585 (2.67°C).

The Suez station showed a distinct tendency from the other ERSC stations under study, which is related to the Mediterranean Sea depression (also known as the Cyprus depression) and the attraction of subtropical streams, whereas the other ERSC stations were impacted by tropical streams.

The present work is considered the first attempt to statistically downscale the future T2m along the ERSC. The current result together with previously dynamical downscaling results (**Elbessa *et al.*, 2021**) especially in the Suez Gulf enriches the uncertainty analysis of the future climate. Moreover, the authors are willing to expand the studied statistical tool to cover the ERSC. Finally, the current research sheds light on the importance of studying the effect of climate change on the coastal zone, industrial, and tourism sectors.

In future studies, the authors will expand the current work to study new stations distributed throughout the ERSC to obtain a full picture of the future uncertainties in the ERSC. Moreover, the use of a regional climate model as a scientific tool for dynamical downscaling merits our attention in future work.

We are now able to better understand the science behind climate change, better analyze the current atmospheric characteristics, and better model the future to support addressing the causes and consequences of climate change.

REFERENCES

- **Anagnostou E. N.; Negri A. J. and Adler R. F. (1999)**. Statistical adjustment of satellite microwave monthly rainfall estimates over Amazonia, *J. Appl. Meteorol.*, 38: 1590-1598.
- **Bawadekji, A.; Tonbol, K.; Ghazouani, N.; Becheikh, N. and Shaltout, M. (2022)**. Recent atmospheric changes and future projections along the Saudi Arabian Red Sea Coast. *Scientific Reports*, 12(1). <https://doi.org/10.1038/s41598-021-04200-z>

- **Chaidez, V.; Dreano, D.; Agusti, S.; Duarte, C. M. and Hoteit, I. (2017).** Decadal trends in Red Sea maximum surface temperature. *Scientific Reports*, 7(1). <https://doi.org/10.1038/s41598-017-08146-z>
- **Calvin, K.; Dasgupta, D.; Krinner, G.; Mukherji, A.; Thorne, P. W.; Trisos, C.; Romero, J.; Aldunce, P.; Barrett, K.; Blanco, G.; Cheung, W. W. L.; Connors, S.; Denton, F.; Diongue-Niang, A.; Dodman, D.; Garschagen, M.; Geden, O.; Hayward, B.; Jones, C. and Ha, M. (2023).** *IPCC, 2023: Climate Change 2023: Synthesis Report. Contribution of Working Groups I, II and III to the Sixth Assessment Report of the Intergovernmental Panel on Climate Change [Core Writing Team, H. Lee and J. Romero (eds.)]. IPCC, Geneva, Switzerland.* (P. Arias, M. Bustamante, I. Elgizouli, G. Flato, M. Howden, C. Méndez-Vallejo, J. J. Pereira, R. Pichs-Madruga, S. K. Rose, Y. Saheb, R. Sánchez Rodríguez, D. Ürge-Vorsatz, C. Xiao, N. Yassaa, J. Romero, J. Kim, E. F. Haites, Y. Jung, R. Stavins, ... C. Péan, Eds.). <https://doi.org/10.59327/IPCC/AR6-9789291691647>
- **Dunne, J. P.; John, J. G.; Adcroft, A. J.; Griffies, S. M.; Hallberg, R. W.; Shevliakova, E.; Stouffer, R. J.; Cooke, W.; Dunne, K. A.; Harrison, M. J.; Krasting, J. P.; Malyshev, S. L.; Milly, P. C. D.; Phillipps, P. J.; Sentman, L. T.; Samuels, B. L.; Spelman, M. J.; Winton, M.; Wittenberg, A. T. and Zadeh, N. (2012).** GFDL's ESM2 global coupled climate-carbon earth system models. Part I: Physical formulation and baseline simulation characteristics. *Journal of Climate*, 25(19): 6646-6665. <https://doi.org/10.1175/JCLI-D-11-00560.1>
- **Dunne, J. P.; Jasmin G. J. and Coauthors. (2013).** GFDL's ESM2 Global Coupled Climate-Carbon Earth System Models. Part II: Carbon System Formulation and Baseline Simulation Characteristics. *Journal of Climate*, Page(s): 2247-2267, DOI: <https://doi.org/10.1175/JCLI-D-12-00150.1>.
- **Eladawy, A.; Nadaoka, K.; Negm, A.; Abdel-Fattah, S.; Hanafy, M. and Shaltout, M. (2017).** Characterization of the northern Red Sea's oceanic features with remote sensing data and outputs from a global circulation model. *Oceanologia*, 59(3), 213-237. <https://doi.org/10.1016/j.oceano.2017.01.002>
- **Elbessa, M.; Abdelrahman, S. M.; Tonbol, K. and Shaltout, M. (2021).** Dynamical downscaling of surface air temperature and wind field variabilities over the southeastern levantine basin, mediterranean sea. *Climate*, 9(10). <https://doi.org/10.3390/cli9100150>
- **Griffies, S.M. and Coauthors. (2011).** The GFDL CM3 coupled climate model: characteristics of the ocean and sea ice simulations. *J. Clim.* 24, 3520-3544, <http://dx.doi.org/10.1175/2011JCLI3964.1>.
- **Hamed, M. M.; Salehie, O.; Nashwan, M. S. and Shahid, S. (2023).** Projection of temperature extremes of Egypt using CMIP6 GCMs under multiple shared socioeconomic pathways. *Environmental Science and Pollution Research*, 30(13), 38063-38075. <https://doi.org/10.1007/s11356-022-24985-4>
- **Hereher, M. E. (2015).** Assessment of Egypt's Red Sea coastal sensitivity to climate change. *Environmental Earth Sciences*, 74(4): 2831-2843. <https://doi.org/10.1007/s12665-015-4304-z>

- **Hersbach, H.; Bell, B.; Berrisford, P.; Hirahara, S.; Horányi, A.; Muñoz-Sabater, J.; Nicolas, J.; Peubey, C.; Radu, R.; Schepers, D.; Simmons, A.; Soci, C.; Abdalla, S.; Abellan, X.; Balsamo, G.; Bechtold, P.; Biavati, G.; Bidlot, J.; Bonavita, M.; ... Thépaut, J. N. (2020).** The ERA5 global reanalysis. *Quarterly Journal of the Royal Meteorological Society*, 146(730): 1999-2049. <https://doi.org/10.1002/qj.3803>
- **Kendall M.G. (1975).** Rank Correlation Methods. New York, NY: Oxford University Press.
- **Mann H.B. (1945).** Non-parametric test against trend, *Econometrica* 13: 245-259. doi: 10.2307/1907187
- **Michel, D.; Pandya, A. A.; Henry L. Stimson Center.; Henry L. Stimson Center. Regional Voices. and Regional Centre for Strategic Studies (Colombo, S. L. (2010).** *Coastal zones and climate change: risk and response*. Henry L. Stimson Center.
- **Moustafa, F. M. and Gerges, M. A. (1994).** *Implications of Climate Change in the Red Sea and Gulf of Aden Region: An Overview UNEP Regional Seas Reports and Studies No. 156* " <https://wedocs.unep.org/20.500.11822/11789>.
- **Reichle R. H. and Koster, R. D. (2004).** Bias reduction in short records of satellite soil moisture. *Geophys. Res. Lett.*, 31, L19501. 10.1029/2004GL020938.
- **Tonbol, K.M.; El-Geziry, T.M. and Elbessa, M. (2019).** Assessment of weather variability over Safaga harbour, Egypt. *Arabian Journal of Geosciences*. 12 (24), 805. <https://doi.org/10.1007/s12517-019-4974-z>
- **United Nations Development Programme. (2005).** *Human development report 2005: international cooperation at a crossroads: aid, trade and security in an unequal world*. [Oxford University Press].
- **Wang, F.; Shao, W.; Yu, H.; Kan, G.; He, X.; Zhang, D.; Ren, M. and Wang, G (2020).** Re-evaluation of the Power of the Mann-Kendall Test for Detecting Monotonic Trends in Hydrometeorological Time Series. *Frontiers in Earth Science*, 8, 14. <https://doi.org/10.3389/feart.2020.00014>
- **Wood A. W.; Maurer E. P.; Kumar A. and Lettenmaier D. P. (2002).** Longrange experimental hydrologic forecasting for the eastern United States, *Journal of Geophysical Research*, 107(D20), 4429, doi:10.1029/2001JD000659.
- **Williamson, D.; Parker, RA. and Kendrick, Juliette. (1989).** The box plot: A simple visual method to interpret data. *Annals of internal medicine*. 110. 916-21. 10.1059/0003-4819-110-11-916.